MotiQ: an open-source toolbox to quantify the cell motility and morphology of microglia

Jan N. Hansen[1,2*], Matthias Brückner[2], Marie J. Pietrowski[1], Jan F. Jikeli[3], Monika Plescher[1,2], Hannes Beckert[1,2], Mareike Schnaars[2], Lorenz Fülle[4], Katharina Reitmeier[5], Thomas Langmann[5], Irmgard Förster[4], Delphine Boche[6], Gabor C. Petzold[1,7], and Annett Halle[1,2,8*]

[1]German Center for Neurodegenerative Diseases (DZNE), Bonn, Germany

[2]Max-Planck research group Neuroimmunology, Research center caesar, Bonn, Germany

[3]Minerva research group Molecular Physiology, Research center caesar, Bonn, Germany

[4]Immunology and Environment, Life and Medical Sciences (LIMES) Institute, University of Bonn, Bonn, Germany

[5]Laboratory for Experimental Immunology of the Eye, Department of Ophthalmology, University Hospital of Cologne, Cologne, Germany

[6]Clinical Neurosciences, Clinical and Experimental Sciences, Faculty of Medicine, University of Southampton, Faculty of Medicine, Southampton, United Kingdom

[7]Department of Neurology, University Hospital Bonn, Germany

[8]Department of Neuropathology, University Hospital Bonn, Germany

* Corresponding authors

Running head: MotiQ - quantifying images of microglia

Abbreviations: 2D, two-dimensional; 3D, three-dimensional; ATP, adenosine triphosphate; CNS, central nervous system.

Abstract

Microglia are the primary resident innate immune cells of the central nervous system (CNS). They possess branched, motile cell processes that are important for their cellular functions. To study the pathways that control microglial morphology and motility under physiological and disease conditions, it is necessary to quantify microglial morphology and motility precisely and reliably. Several image analysis approaches are available for the quantification of microglial morphology and motility. However, they are either not automated, not freely accessible, and/or limited in the number of morphology and motility parameters that can be assessed. Thus, we have developed *MotiQ*, an open-source, freely accessible software for automated quantification of microglial motility and morphology. *MotiQ* allows quantification of a diverse set of cellular motility and morphology parameters, including the parameters that have become gold standard in the microglia field. We demonstrate that *MotiQ* can be applied to *in vivo*, *ex vivo,* and *in vitro* data from confocal, epifluorescence, or two-photon microscopy and we compare its results to other analysis approaches. We suggest *MotiQ* as a versatile and customizable tool to study microglia.

Brief

MotiQ is an open-source software for automated quantification of microglial motility and morphology. *MotiQ* can be applied to *in vivo*, *ex vivo*, and *in vitro* data from confocal, epifluorescence, or two-photon microscopy. *MotiQ* is not limited to microglia - it can also be applied to other cell types.

Introduction

Microglia are the parenchymal tissue resident macrophages of the central nervous system. In the intact adult brain, microglia are highly ramified and have a complex three-dimensional

(3D) branch structure. Intravital two-photon microscopy in mice with microglia-specific expression of enhanced green fluorescence protein has shown that microglial cell branches are highly motile and continuously undergo extension and retraction (Davalos *et al.*, 2005; Nimmerjahn *et al.*, 2005). This motility enables microglia to perform the surveillance of their environment to then execute their functions, including limiting synaptic excitability (Badimon *et al.*, 2020), partial phagocytosis of synaptic structures (Weinhard *et al.*, 2018), synaptic pruning during development and in disease (Hong *et al.*, 2016), and formation and maintenance of synapses (Miyamoto *et al.*, 2016). It has been estimated that the cortical parenchyma is completely scanned by microglia every few hours (Nimmerjahn *et al.*, 2005).

Microglial morphology and motility change during systemic inflammation (Gyoneva *et al.*, 2014), in neurodegenerative and neuropsychiatric diseases (Bolmont *et al.*, 2008; De Picker *et al.*, 2021; Franco-Bocanegra *et al.*, 2021), upon aging (Conde and Streit, 2006; Hefendehl *et al.*, 2014), and in response to specific deletions of microglial receptors (Pagani *et al.*, 2015; Sipe *et al.*, 2016; Madry *et al.*, 2018; Merlini *et al.*, 2021). To study the pathways that underlie these changes and to determine their functional impact, it is necessary to precisely and reliably analyze microglial cell motility. Over the past years, a set of parameters for microglial morphology has become standard, such as the surface area to volume ratio (e.g., (Orr *et al.*, 2009; Madry *et al.*, 2018; Plescher *et al.*, 2018)), the total length of the process tree as well as the numbers of branches and tips (e.g., (Nimmerjahn *et al.*, 2005; Hefendehl *et al.*, 2014; Erny *et al.*, 2015)), or the convex hull around the cell (e.g., (Fontainhas *et al.*, 2011; Baron *et al.*, 2014; Fernández-Arjona *et al.*, 2017)). Current analysis approaches (i) are only partly automated (Fernández-Arjona *et al.*, 2017; Young and Morrison, 2018), provide low throughput, (ii) rely on manual tracing of cells (Cătălin *et al.*, 2017; Paris *et al.*, 2018; Basilico *et al.*, 2019; Sun *et al.*, 2019),

(iii) are limited to a two-dimensional (2D) analysis (Cătălin *et al.*, 2017; Fernández-Arjona *et al.*, 2017; Kluge *et al.*, 2017; Madry *et al.*, 2018; Young and Morrison, 2018; Kyria zis *et al.*, 2019), and/or (iv) use custom-written lab-specific software, with which a limited number of microglial parameters can be determined (Abdolhoseini *et al.*, 2016; Kluge *et al.*, 2017; Madry *et al.*, 2018; Paris *et al.*, 2018; Kyriazis *et al.*, 2019). Commercial image analysis software such as Imaris (Bitplane) has been used in previous studies, but these commercial solutions are not available to every lab due to cost considerations, and often use proprietary algorithms.

Here, we introduce *MotiQ*, a versatile and open-source software for the automatized and comprehensive quantification of microglial motility and morphology in 2D and 3D microscopic image series. In addition to data from two-photon microscopy, *MotiQ* is applicable to a variety of other microscopic data sets and allows for the quantification of a broad set of over 60 parameters of microglial morphology, motility and signaling. *MotiQ* is a freely-accessible resource for microglia research and represents an open-source platform for researchers to establish standards for microglial quantification.

Results

MotiQ workflow

We primarily developed *MotiQ* to quantify microglial morphology and motility in 3D time-lapse images acquired by *in vivo* two-photon microscopy. For open access and high applicability *MotiQ* is composed of modular ImageJ plugins. The source code, all plugins, and a manual are freely accessible online (https://github.com/hansenjn/MotiQ). *MotiQ* allows two types of analyses: a more rapid 2D analysis of maximum-intensity projections (Fig. 1a), and a more comprehensive analysis of original 3D z stacks (Fig. 1b). Both *MotiQ* quantification approaches are performed with a three-step workflow using the plugins (1) *MotiQ cropper* for

single-cell image generation, (2) *MotiQ thresholder* for image segmentation, and (3) *MotiQ 2D analyzer* or *MotiQ 3D analyzer* for quantification. This three-step plugin format allows to replace or adapt individual steps, to include additional plugins in the workflow, or to use individual *MotiQ* plugins for applications other than microglial cell analysis.

The first plugin, *MotiQ cropper*, aids in the selection of single microglia from recordings, and generates images comprising one individual microglial cell (for technical details see Supplementary Note 1 and the Manual provided on the GitHub page). We implemented this user-dependent single-cell selection approach to realize the analysis of microglia under pathological conditions, e.g., Alzheimer's disease (AD), where microglia and their cell processes are densely packed and closely interlaced at cell border (Condello *et al.*, 2015), which renders automated single-cell detection imprecise. This challenge is commonly addressed by manual tracing approaches, in which a trained investigator traces the individual processes of a single cell, which can be time consuming (Gyoneva and Traynelis, 2013; Baron *et al.*, 2014; Cătălin *et al.*, 2017; Paris *et al.*, 2018; Basi lico *et al.*, 2019; Sun *et al.*, 2019). In contrast, in *MotiQ* cropper a region of interest (ROI) that contains an individual cell is selected. The cell detection and process tracing itself is then fully automated based on the other *MotiQ* plugins. The single cell selection with *MotiQ* is therefore faster than careful manual tracing, since the user does not need to precisely track individual processes but only needs to roughly encircle a ROI. Additionally, by guiding the user through z stacks and time frames, by transferring selections from image to image, and by automatically saving the resulting single-cell image and metadata pertaining to the selected regions of interest (ROIs), *MotiQ cropper* renders the whole process more time-efficient. The output image, together with corresponding metadata, can be used to retrospectively validate the selection process.

The next step in the *MotiQ* workflow is image segmentation, which is accomplished using *MotiQ thresholder* (Supplementary Note 2). In other image analysis methods for microglia, such as multi-step protocols for ImageJ (e.g. (Fontainhas *et al.*, 2011; Fernández-Arjona *et al.*, 2017; Young and Morrison, 2018), users adjust settings and threshold values to segment cells from background, image by image. Such manual multi-step workflows are time-consuming and error-prone, unless fully-automated macros are developed. *MotiQ thresholder* standardizes and automatizes image preprocessing and segmentation, even for users that are not able to develop computer code. *MotiQ thresholder's* pipeline, including image preprocessing steps, local or global auto-threshold methods, and image segmentation, is easily customizable by the user through the plugin's settings dialog.

We implemented image preprocessing steps in *MotiQ thresholder* that allow to produce an image in which foreground (microglia) and background intensities are more distinguished: (1) down-scaling of image resolution, (2) rescaling the intensity histogram for better coverage of the intensity range, (3) including multiple time frames or z stacks into the histogram, and (4) converging the relationship of fore- and background pixel numbers towards equilibrium, e.g., by using maximum-intensity projections of multiple time step or z stack images. The user can select one or a combination of those methods. For a detailed description and illustration of the rationale behind these methods, see Supplementary Note 2 and Supplementary Figures 1 and 2. For subsequent threshold calculation, *MotiQ thresholder* uses one of the intensity thresholding algorithms available in ImageJ. This threshold algorithm to be used is defined by the user, based on the best performance in separating fore- and background in the user's images. Importantly, *MotiQ thresholder* performs image preprocessing and threshold calculation in an automatically generated copy of the image, while the intensity threshold is finally applied to the unsegmented, original input image. Thereby, the preprocessing methods do not result in a loss of resolution or dimension and *MotiQ thresholder* does not only generate a binary image but can also produce a background-removed version of the original

image, containing fully preserved fluorescence intensity information. *MotiQ thresholder* also allows for separate threshold calculation and application in individual time frames, which is important for time-lapse data with instable fluorescence intensity levels, e.g., due to photobleaching. Since the user may need to optimize the *MotiQ thresholder* settings for individual data sets, we provide default settings for the analysis of different types of data in Supplementary Table 1, which may serve as a starting point for further optimizations.

In the last step of the *MotiQ* workflow, cell analysis and visualization are performed using *MotiQ 2D analyzer* or *MotiQ 3D analyzer*, depending on the respective image type (Supplementary Note 3). First, connected pixels are detected and bundled to individual objects via a *Flood-Filler* algorithm. Objects smaller than a pre-defined size are removed, which allows to remove noise pixels, falsely-detected as foreground. The remaining larger objects are considered to belong to the selected microglial cell and are quantified. In this step, the microglial cell, its cell skeleton, and its convex hull are automatically reconstructed from these objects and over 60 cellular parameters that represent microglial morphology (Supplementary Table 2), motility (Supplementary Table 3), and signaling (Supplementary Table 4) are automatically determined. We collected the major part of this list of parameters based on the parameters that have been applied to microglia in the literature and that are considered standard parameters (details below). We aimed to make the application of *MotiQ* as versatile as possible and allow the best comparability of output data to previous literature reports. Furthermore, *MotiQ 3D analyzer* contains a tool that illustrates the analysis results in 3D visualizations (Figure 1a).

Analysis of in vivo and ex-vivo two-photon microscopy data sets

To demonstrate which microglial morphology and dynamic parameters can be determined with *MotiQ*, we subjected recordings from intravital time-lapse two-photon microscopy in

CX3CR1-EGFP/wt mice (Jung *et al.*, 2000) to the *MotiQ* 2D and 3D analysis workflow (Supplementary Videos 1-2).

The morphology of a microglial cell is predominantly characterized by its ramification, i.e., the complexity of its branch structure. Microglial ramification is measured by two main approaches: (1) by determining the relationship of cell surface to cell volume (ramification index) (e.g. (Orr *et al.*, 2009; Madry *et al.*, 2018; Plescher *et al.*, 2018)) and (2) by analyzing the microglial cell skeleton (e.g., (Nimmerjahn *et al.*, 2005; Hefendehl *et al.*, 2014; Erny *et al.*, 2015)). The ramification index describes the overall complexity of the microglial cell and the cell skeleton parameters provide additional information about subcomponents of the microglial process tree.

More specifically, the 2D ramification index is defined as the ratio of the cell contour to the circumference of a circle with the same cell area as the respective cell (Fig. 2a) and the 3D ramification index is defined as the ratio of the cell surface area to the surface area of a sphere with the same volume as the respective cell (Fig. 2b). For skeletonization and analysis of the resulting cell skeleton, we implemented the ImageJ plugins *Skeletonize3D* and *AnalyzeSkeleton* (Arganda-Carreras *et al.*, 2010) in *MotiQ*, allowing to quantify a variety of cell skeleton characteristics (Supplementary Table 2), including number of tips, number of branches, and total tree length (Figure 2c and d). Other morphological parameters that are included in *MotiQ* are the brain area (2D) or brain volume (3D) spanned by a microglial cell, i.e., spanned area (Fig. 2e) or spanned volume (Fig. 2f), which are defined as the size of the cell's convex hull and represent the territory of an individual cell. Thus, these parameters reveal the potential influence of the microglial cell on the surrounding brain parenchyma. As a measure for cell polarity i.e., the asymmetric distribution of processes from the soma, the vector from the cell's center of mass to the center of the convex hull is included in *MotiQ* (Fig. 2e and f).

In addition to morphological parameters, we included parameters in *MotiQ* that represent dynamic changes of the microglial cell and its process tree. For example, *MotiQ* allows determining the number and area (2D) or volume (3D) of individual microglial process extensions and retractions in consecutive time steps (Fig. 2g and h). Individual extensions or retractions are defined as objects consisting of a group of connected pixels that newly emerge or disappear in an image compared to the previous time step. The parameter *shape dynamics* is the sum of the total extended and retracted area (2D) or volume (3D) and serves as a measure for the overall change of the microglial cell shape. Furthermore, as a read-out for the interaction of a microglial cell with its environment, *MotiQ* allows to determine the scanned area (2D, Fig. 2i) or scanned volume (3D, Fig. 2j), which are defined as the brain area or the brain volume that is occupied by a microglial cell and its processes over a longer time span. A similar parameter, called "volume fill", has been applied in 2D before (Nimmerjahn *et al.*, 2005) for a whole stack of images containing many cells, demonstrating that microglial motility allows microglia to sample the brain volume over time. We introduce this parameter for single cells as a measure for microglial scanning activity and add that the scanned area or volume is subdivided into the static area or volume, in which the cell is present in all analyzed time frames (usually the soma and larger primary cell branches), and the dynamic area or volume, in which the cell compartment is only transiently present (Fig. 2i and 2j). The scanning activity of the cell is determined as the percentage of the scanned area or volume that is dynamic.

To test whether *MotiQ* sensitively detects changes in morphology and motility, we next analyzed microglia before and after stimulation in *ex-vivo* time-lapse two-photon microcopy recordings from acute cerebral slices with *MotiQ*. Acute slice preparations have been used to study microglial responses to extracellular stimuli such as extracellular adenosine triphosphate (ATP) (Fontainhas *et al.*, 2011; Dissing-Olesen *et al.*, 2014; Matyash *et al.*, 2017). We perfused cerebral slices with ATP to induce a

change in microglial morphology and motility. We then analyzed the microscopic data with *MotiQ 2D* and *3D* (Fig. 3). We sensitively and reliably detected ATP-induced changes in morphology and dynamic parameters, such as an increase in the ramification index (Fig. 3c and d), number of branches, tree length (Fig. 3e and f), spanned area (2D, Fig. 3g) or volume (3D, Fig. 3h), shape dynamics (Fig. 3i-j), and microglial scanning parameters (Fig. 3i-l).

Analysis of histological data sets

Since morphometric end-point analysis of microglia in fixed tissue is one of the most commonly used techniques in microglia research, we next analyzed confocal images of immuno-fluorescently labeled Iba1-positive murine microglia in fixed cerebral (Fig. 4a-d) and retinal (Fig. 4e-h) tissue sections. For both data sets, we used *MotiQ* to reconstruct microglia and analyze their morphological characteristics. To further illustrate the range of applications of *MotiQ*, we additionally analyzed confocal images of immuno-fluorescently GFAP-positive astrocytes (Fig 4i-l) and Iba1-positive human microglia (Fig. 4m-p). Here we show that *MotiQ* could be also used to analyze a broad range of other cell types.

Fully-automated analysis of histological data sets

MotiQ 3D Analyzer can automatically separate microglial cells without user-dependent cell selection by *MotiQ cropper*. This is, however, only reliably applicable to high-resolution 3D microscopy data with a high stack depth, as in these data sets, cells next to each other can be clearly separated and there are cells that are completely inside the stack so that their entire process tree can be continuously reconstructed. To demonstrate the high-throughput *MotiQ* analysis, we subjected a whole confocal image of immuno-fluorescently labeled Iba1-positive murine microglia in fixed cerebral tissue sections to the *MotiQ* workflow without *MotiQ Cropper* (Fig. 5 a). In this workflow, *MotiQ 3D Analyzer* was set to track all particles by overlap in the image and analyze each particle separately (see Supplementary Note 3). Indeed, *MotiQ* could user-independently separate and reconstruct individual cells in the stack (Fig.

5b) and revealed their morphological characteristics (Fig. 5c). To scrutinize the validity and accuracy of this approach, we also subjected the same data set to two other established methods for quantifying microglial morphology: (1) An automated analysis approach based on the commercial software Imaris (Fig. 5d) (Gyoneva and Traynelis, 2013; Gyoneva *et al.*, 2014; Hefendehl *et al.*, 2014) and (2) a manual tracing of the individual cells (Baron *et al.*, 2014; Cătălin *et al.*, 2017; Basilico *et al.*, 2019; Sun *et al.*, 2019) based on the Simple Neurite Tracer plugin for Fiji (Longair *et al.*, 2011; Arshadi *et al.*, 2021) (Fig. 5d). Of note, approach 2 required a trained observer about 30 minutes of user interaction per cell. Importantly, the resulting output parameters significantly correlated with the respective *MotiQ* parameters (Fig. 5d, e), showing that *MotiQ* output parameters are qualitatively comparable to these other approaches.

Analysis of *in vitro* live-cell data sets

Next, we tested whether *MotiQ* can be applied to data sets from cultured microglia. The morphology and motility of cultured murine or human microglia can be imaged in a 2D culture system on plastic or glass surface (Honda *et al.*, 2001; Koizumi *et al.*, 2007) or using 3D culture systems, in which microglia are cultured in a 3D matrix, such as Matrigel (Orr *et al.*, 2009) or collagen (Haw *et al.*, 2014), in co-culture with other CNS cells (Takata *et al.*, 2017) or in cerebral organoids (Ormel *et al.*, 2018). Here, we acquired time-lapse images of GFP-positive murine primary microglia in a 2D culture system using epifluorescence microscopy, and in a 3D Matrigel culture system using spinning disc confocal microscopy. We added ATP during the imaging experiments to induce changes in microglial morphology and motility.

We subjected the data set of each experimental design to the *MotiQ 2D* or *3D* analysis workflow (Fig, 6; Supplementary Videos 3-4). Here, we selected slightly adapted *MotiQ*

thresholder settings for optimized image segmentation (Supplementary Table 1). Again, with *MotiQ* we sensitively detected experimentally-induced changes in microglial morphology and motility, i.e., in cell polarity (Fig. 6c and i), shape dynamics (Fig. 6d and k), and scanning activity (Fig. 6e and l). Of note, directionality parameters (Fig. 6m and f) are also implemented in *MotiQ* and can be used when studying chemokinesis or chemotaxis.

Since the image segmentation step in *MotiQ* fully preserves fluorescence intensity information of the cell, *MotiQ* can also be used to quantify cellular fluorescence intensity levels, kinetics, and distribution. This allows for a direct correlation of microglial morphology and dynamics with cellular fluorescence parameters. As more chemical and genetically encoded fluorescent indicators become available for signaling molecules such as protons, calcium or second-messengers, *MotiQ* can be used for studying signaling pathways that underlie cellular morphology and motility. To demonstrate such correlative measurements of morphology, motility and fluorescence kinetics, we generated time-lapse images of primary murine macrophages expressing the genetically-encoded calcium sensor GCaMP3 during high-dose ATP treatment (5 mM). We then analyzed an exemplary data set using *MotiQ* (Supplementary Video 5), which revealed a temporal correlation of a transient intracellular/cytosolic calcium increase (Fig. 7a) with changes in macrophage ramification (Fig. 7b) and scanning activity (Fig. 7c) during ATP perfusion.

Analysis of microglia in a mouse model of Alzheimer's disease

Finally, we assessed the applicability and accuracy of *MotiQ* on a bench-mark data set. We chose to analyze the morphology and motility of microglia in the APP/PS1 mouse model of AD (Jankowsky *et al.*, 2003). It has previously been shown that microglia in AD mouse models show reduced ramification and motility (Bolmont *et al.*, 2008; Koenigsknecht-Talboo *et al.*, 2008; Krabbe *et al.*, 2013; Plescher *et al.*, 2018) in particular when in vicinity to Abeta plaques (Bolmont *et al.*, 2008; Plescher *et al.*, 2018). Thus, we aimed to test whether

MotiQ can reliably reveal these pathological changes, as well. We obtained acute cerebral slices from APP/PS1 CX3CR1-EGFP/wt mice and "wild-type" CX3CR1-EGFP/wt mice, acquired images with a two-photon microscope (Fig. 8a and b), and subjected them to *MotiQ* analysis. *MotiQ* 3D analysis revealed a significant reduction of ramification (Fig. 8c) and tree length (Fig. 8d) in plaque-associated and plaque-distant microglia, while plaque-associated microglia were mostly affected, in line with previous reports in another AD mouse model (Plescher *et al.*, 2018). Similarly, *MotiQ* analysis revealed impaired microglial motility in APP/PS1 CX3CR1-EGFP/wt mice, especially at the plaque, reported by the *MotiQ* parameters shape dynamics (Fig. 8e) and scanned area (Fig. 8f). We next sought to compare these results to a previously decribed manual approach for quantifying microglial motility (Nimmerjahn *et al.*, 2005; Bolmont *et al.*, 2008): A trained observer tracked the position of individual microglial process tips manually for all cells. This showed that process extensions and retractions were slower in the AD mouse model, especially at the plaque (Fig. 8g and h). Importantly, the results from manual tracking correlated with the motility parameters determined with *MotiQ* analysis (Fig. 8i and j).

Discussion

Due to the paucity of freely accessible and easy-to-use standard tools for image analysis of microglia, approaches for the quantification of microglial morphology and dynamics have largely varied between studies to date, making comparison of data difficult. To fill this gap, we developed the open-source ImageJ-based software *MotiQ* that enables the quantification of more than 60 parameters of microglial morphology, motility, and fluorescence kinetics. We furnished *MotiQ* with a modular structure so that each individual *MotiQ* plugin can be potentially used for different approaches. For example, *MotiQ thresholder* is a flexible tool for image preprocessing and segmentation that offers a variety of thresholding approaches.

MotiQ thresholder automatizes image preprocessing and segmentation workflows, fosters reproducibility by logging the individual image preprocessing and segmentation steps, and is readily applicable to other data and workflows.

In *MotiQ* we integrated several parameters that have become standard for the quantification of microglial morphology and motility to allow the best comparability of output data to previous studies. For example, the parameter *ramification index*, which describes the overall complexity of a microglial cell, has previously been used by us (Fülle *et al.*, 2018; Plescher *et al.*, 2018; Schmöle *et al.*, 2018) and others and is similar to the described parameters surface area-to-volume ratio (Orr *et al.*, 2009; Gyoneva and Traynelis, 2013) or cell circularity (Fernández-Arjona *et al.*, 2017). Parameters that characterize the microglial process tree have been previously used in several studies to quantify microglial morphology changes (Fontainhas *et al.*, 2011; Baron *et al.*, 2014; Hefendehl *et al.*, 2014; Erny *et al.*, 2015; Catalin *et al.*, 2017; Kluge *et al.*, 2017; Fulle *et al.*, 2018; Plescher *et al.*, 2018). The parameters *spanned area* (2D) or *spanned volume* (3D) that focus on the interaction of the microglial cell with its environment, have been used in custom-written analysis approaches (Fontainhas *et al.*, 2011; Baron *et al.*, 2014; Fernández-Arjona *et al.*, 2017). In previous studies the number of process extensions and retractions (Koenigsknecht-Talboo *et al.*, 2008) or the speed of single processes (Davalos *et al.*, 2005; Nimmerjahn *et al.*, 2005; Bolmont *et al.*, 2008; Gyoneva *et al.*, 2014; H efendehl *et al.*, 2014; Paris *et al.*, 2018) have been – mostly manually – quantified as an important parameter of dynamic behavior of microglia. With *MotiQ* the number and extent of individual process extensions and retractions are automatically determined, similar to previous custom-written analysis approaches for microglial motility (Kluge *et al.*, 2017; Madry *et al.*, 2018), which, however, were limited to 2D analysis, in contrast to *MotiQ*, which provides a 3D implementation. Of note, we show that *MotiQ's*

parameters for microglial morphology and motility directly correlate to results from manual process tracking, highlighting that *MotiQ* can automatize the manual tracking of processes while revealing functionally similar results.

As novel dynamic parameters, we implemented *scanning activity* (2D/3D), *scanned area* (2D), and *scanned volume* (3D) in *MotiQ* to quantify the brain volume that is sampled by an individual microglial cell. Moreover, *MotiQ* offers parameters that describe the directionality of cellular movement, which are important when measuring the chemotactic response of microglia towards stimuli, especially in *in vitro* experiments, but potentially also *in vivo*. Importantly, *MotiQ* enables correlative studies on morphology, dynamics, and fluorescence kinetics in a cell to address the role of cellular signaling pathways using fluorescent indicators such as calcium- or pH-sensitive dyes.

MotiQ can be applied to a variety of data sets, including *in vivo* and *ex vivo* two-photon microscopy of microglia, confocal end-point analysis of microglial morphology in fixed tissue sections, and epifluorescence and confocal live-cell microscopy of cultured microglia. Of note, in high-resolution images, where adjacent microglial process can be clearly separated, *MotiQ* could fully automatically reconstruct microglial cells without any user-dependent cell selection, while revealing similar results compared to a time-consuming manual analysis. Thus, under these conditions, MotiQ allows analyzing microglial morphology with high throughput and thereby, performing detailed morphological studies on microglia with high statistical power.

Furthermore, *MotiQ* is not restricted to study murine or human microglia, but could also be used to characterize other glial cells such as astrocytes, or the dynamics of subcellular structures, such as neuronal growth cones or primary cilia.

The only comparable widely used alternative for studying microglial morphology and dynamics is the commercial software Imaris. However, Imaris is not affordable for every lab

and the underlying code and algorithms are not freely available. In contrast, the source code of *MotiQ* is freely accessible (https://github.com/hansenjn/MotiQ), making the analysis procedure transparent and customizable.

MotiQ offers a precise and comprehensive analysis of microglial morphology and motility. We envision that *MotiQ* will become a tool in microglial research used by many labs, fostering comparability of data and facilitating investigations on pathways controlling microglial morphology and the interaction of microglia with their environment.

Materials and Methods

Animals

Lifeact–GFP (Clausen *et al.*, 1999; Riedl *et al.*, 2010), LysMcre (Clausen *et al.*, 1999), Ai38GCaMP (Zariwala *et al.*, 2012), APP/PS1 (Jankowsky *et al.*, 2003) and CX3CR1$^{EGFP/wt}$ (Jung *et al.*, 2000) mice have been described previously. C57BL/6J mice were purchased from Janvier Labs. CX3CR1$^{EGFP/wt}$ and Ai38-GCaMP mice were purchased from Jackson Laboratories. Lifeact-GFP mice were provided by Frank Bradke (DZNE, Bonn, Germany) with permission of Michael Sixt (IST, Austria). Mice were housed in groups on a 12-h light/dark cycle with food and water available *ad libitum*. Research and animal care procedure were approved by the Animal Care Committee of the district government.

Human brain tissue

Post-mortem tissue samples from a non-neurological non-neuropathological 62-year-old control case were obtained from the University Hospital Southampton NHS Foundation Trust as part of the UK Brain Archive Information Network (BRAIN UK), which is funded by the Medical Research Council and Brain Tumour Research. The use of human tissue was covered

by the ethical approval provided by BRAIN UK (Research Ethics Committee South Central Hampshire B, reference 14/SC/0098).

In vivo two-photon imaging

CX3CR1$^{EGFP/wt}$ mice were anesthetized with isoflurane (1.5-3% in 100% oxygen at 0.7-1 l min^{-1}). Body temperature was kept at 37°C. Hair, skin and periosteum were removed and skull was fixed in a custom-made metal frame using a cyano veneer fast/cyano veneer powder mixture (Hager & Werken, Duisburg, Germany). The metal frame was fixed in a custom-made stereotactic device. A cranial window (3 mm diameter) was created using a dental drill, filled with agarose (37°C; 3% in PBS) and sealed with a cover glass (Hugo Sachs). Two-photon imaging of anesthetized CX3CR1$^{EGFP/wt}$ mice was performed with an upright two-photon microscope (Trim Scope; LaVision Biotec, Bielefeld, Germany) equipped with a 20x objective (1.0 NA, Zeiss). EGFP was excited at 870 nm with a Ti:Sapphire laser (Chameleon Ultra II, pumped by an 18 W laser; Coherent) and scanned at 516-556 nm. Laser power below the objective was 10-20 mW. Image frame rate was 1.6 s at a resolution of 993x993 pixels. Image stacks were recorded starting at ~40 µm below the pial surface of the cortex (36 s intervals, z stack size 60 µm with z slice intervals of 3 µm).

Ex vivo two-photon imaging of acute cerebral slices

CX3CR1$^{EGFP/wt}$ mice were sacrificed and decapitated and brains were immediately transferred to ice-cold aCSF (NaCl 134 mM; KCl 2.5 mM; $MgCl_2$ 1.3 mM; $CaCl_2$ 2 mM; K_2HPO_4 1.26 mM; $NaHCO_3$ 26 mM, D-glucose 10 mM; pH 7.4; saturated with carbogene). Serial coronal cerebral sections (300 µm) were prepared using a Leica VT1200S vibratome (speed: 0.1 mm/s; amplitude: 1.5 mm). Acute slices were fixed in a custom-built perfusion chamber using a harp slice grip (ALA scientific instruments) and perfused at a speed of 1.5 ml/min with aerated aCSF. Imaging was performed using the same two-photon system as described above. Image stacks were recorded starting 20 µm below the coronal surface of the acute cerebral

slice (30.8 s stack intervals, Z stack size 60 µm with z slice intervals of 3 µm). After recording for 10 minutes, 100 µM ATP (Sigma-Aldrich) dissolved in aCSF was washed in for 40 minutes. Finally, ATP was washed out for 10 minutes.

Preparation, staining and imaging of fixed tissue sections

For visualization and analysis of cortical microglia, brains of 8 month-old mice (C57BL6J/C3HHeJ) were immersion-fixed in 4% PFA and microglia were stained in 100 µm thick coronal cryosections with anti-Iba1 (Wako; 019-19741; 1 µg/ml) and goat anti-rabbit Alexa Fluor® 488 (Invitrogen; 3 µg/ml). Confocal imaging was performed with a Nikon Ti-E Confocal Microscope (Nikon, Tokyo, Japan; z stack size 40 µm with z slice intervals of 1 µm, Fig. 4a) or with a Zeiss LSM 700 Confocal Microscope (Carl Zeiss, Germany; z stack size 20 µm with z slice intervals of 0.5 µm, Fig. 5). Astrocytes were visualized in 40 µm thick sagittal vibratome sections from 8-12 week-old mice (C57BL/6J-RCCHsd). Astrocytes were stained in free-floating sections with anti-GFAP (Abcam; ab7260; 1:500) and goat anti-rabbit Alexa Fluor® 594 (Invitrogen; 4 µg/ml) and imaged with a Zeiss LSM 780 Confocal Microscope (Carl Zeiss AG, Oberkochen, Germany; z stack size 30-40 µm with z slice intervals of 1 µm). For analysis of retinal microglia, eyes of 3 month-old C57BL/6J mice were enucleated, fixed and stained as described previously[23]. Retinal whole mounts were imaged using an AxioImager.M2plus ApoTome2 microscope (Carl Zeiss, Germany).

For visualization of human microglia, 50-µm-thick formalin-fixed paraffin-embedded sections from a post-mortem sample of human temporal cortex were incubated with anti-Iba1 (Wako; 019-19741; 1:500) for 24 hours after heat retrieval and subsequently incubated with goat anti-rabbit Alexa Fluor® 488 (Invitrogen; 1:200, 2h), followed by 70% Sudan Black incubation to reduce autofluorescence. Counterstaining was obtained with SYTOX Orange (Invitrogen; 25 nM). Confocal images were generated in the grey matter using a Leica TCS

SP8 laser scanning confocal microscope system equipped with a 63x objective, using a 3.0x digital zoom. Z stacks were acquired with a z-slice interval of 0.5 µm.

Primary microglia

Primary mixed glial cultures were generated to obtain cultured microglia as described[24]. Briefly, newborn CX3CR1$^{EGFP/wt}$ or Lifeact–GFP$^{+/-}$ mice were decapitated. Brains were removed and stripped of their meninges. Brains were mechanically dissociated after incubation with Trypsin-EDTA (0.05%) and cultivated in PLL-coated culture flasks in DMEM (Life Technologies, Darmstadt, Germany; supplemented with 10% FBS (Biochrom, Berlin, Germany) and 1% Penicillin/Streptomycin (Life Technologies, Darmstadt, Germany). After 5-7 days, proliferation of microglia was stimulated by adding supernatant of the murine fibroblastic cell line L929.

Epifluorescence imaging of primary microglia in a 2D culture system

Microglia were obtained from the culture supernatant of primary mixed glial cultures after vigorous shaking and seeded on PLL-coated 8-well plates (Ibidi, Munich, Germany) in phenol red-free and FBS-free DMEM (Life Technologies, Darmstadt, Germany; supplemented with 1 % glutamate, 1 % pyruvate, 1 % penicillin/streptomycin). Cells were imaged at 37°C and 10 % CO_2 using an epifluorescence microscope (Nikon Ti-E, Nikon, Tokyo, Japan) equipped with a 20x objective (Nikon, Tokyo, Japan; NA 0.7) and an EGFP filter set (AHF Analysetechnik, Tübingen, Germany).

Spinning-disk confocal imaging of primary microglia in a 3D culture system

Phenol red-free Corning® Matrigel® Matrix (VWR, Radnor, Pennsylvania) was thawed and placed on top of 5 mm cover slips (gel thickness ~100 µm). After solidification of gel at 37°C (20-30 min), microglia (in DMEM, 10% FBS, 1% Penicillin/Streptomycin) obtained from primary mixed glial cultures of Lifeact–GFP$^{+/-}$ mice, were put on top of the gel in order to

enter the gel. During imaging, the prepared cover slips were continuously perfused with HBSS buffer. Imaging was performed with a spinning disk confocal microscope (Olympus, Tokyo, Japan; 60x objective; time interval 30 s; z stacks 25-35 µm with z slice intervals of 1 µm). After 5 min of baseline recording, perfusion buffer was switched to HBSS containing 100 µM ATP (Sigma Aldrich) for 5 min and then switched again to pure HBSS for 5 min.

Primary bone marrow-derived macrophage cultures

Tibia and femur of heterozygous Ai38-GCaMP:LysMcre mice were prepared and bone marrow was washed out and collected in RPMI medium. After lysis of blood cells, cell pellet was resuspended in 5 ml RPMI, passed through a 40 µm cell strainer and cultivated in RPMI medium containing 10 % FBS and 1 % penicillin/streptomycin at 37°C and 5 % CO_2. Cells were used for experiments after DIV10.

Epifluorescence imaging of primary macrophages

Ai38-GCaMP-positive bone marrow-derived macrophages were seeded on glass cover slips 1 day before experiments. Imaging was performed at room temperature and a gravity-driven perfusion system was used for continuous perfusion with a flow rate between 0.5 - 1 ml/min. Images were acquired every 2 s with a 20x objective (Nikon, Tokyo, Japan; NA 0.7) using an epifluorescence microscope (Nikon Ti-E, Nikon, Tokyo, Japan) equipped with an EGFP filter set (AHF Analysetechnik, Tübingen, Germany) at room temperature. A focus system (Nikon PFS, Nikon, Tokyo, Japan) was used to correct z drift.

Image pre-processing

Epifluorescence microscopy images of microglia in a 2D culture were pre-processed by Bleach Correction using the ImageJ plugin *CorrectBleach* by Kota Miura (correction method: histogram matching). Time-lapse images were registered using the ImageJ plugin *MultiStackReg*[25]. 3D images were intensity-normalized in the z direction using the ImageJ

function *Enhance contrast* (0.5 %; normalized). All images were pre-processed using the ImageJ function *Smooth* with two exceptions: (1) The confocal image of human microglia was pre-processed with *Gaussian Blur* (2 pixel), as it harbored a higher resolution than other images requiring a higher smoothing than performed by the *smooth* function; (2) The confocal image stack of Iba1-labelled microglia that was used for full-automated cell separation of individual microglia was pre-processed using the ImageJ function *Subtract Background* (50 pixel) to reduce regional intensity differences.

***MotiQ* plugins and microglial parameters**

The *MotiQ* analysis workflow is described in the Manual provided via the GitHub repository https://github.com/hansenjn/MotiQ. For a detailed description of all *MotiQ* plugins, see Supplementary Notes 1-4. *MotiQ thresholder* settings for image processing of data shown here are listed in Supplementary Table 1. Microglial morphological, dynamic, and signaling parameters are described in detail in Supplementary Tables 2-4.

Analysis based on Imaris

In Imaris, the surface module was used to select the area covered by microglia (Iba1 channel, smoothing 0.5 µm). To eliminate noise, a manual intensity threshold (18.9338) was applied and a second threshold was adjusted manually to filter for complete cells (> ~30,000 voxels). A mask was created based on the surface and used as input for filament remodeling (7 µm was set as soma size for starting points, 0.5 µm as process diameter for seed points). The thresholds for starting points (28.984) and seed points (110.201) were adjusted manually. Seed points, that were within 14 µm around the starting points and disconnected segments were removed and smoothing (0.1 µm) was applied. In order to obtain continuous processes, an automated maximal gap length (7 µm) was used. The parameters dendrite volume, dendrite area, filament length, number of dendrite branch points, number of dendrite terminal points, number of dendrite segments were chosen to compare to the respective parameter in *MotiQ*

(3D volume, surface, process tree length, number of junctions, number of tips and number of branches).

Manual tracing of the process tree in Fiji using Simple Neurite Tracer

Manual microglial process tracing was performed using the Simple Neurite Tracer plugin in Fiji (Arshadi *et al.*, 2021). All primary branches of a reconstructed cell were combined in a shared root. The skeleton parameters cable length, number of branch points, number of tips and number of branches were used to compare the manual tracing approach to the respective parameters in MotiQ (process tree length, number of junctions, number of tips and number of branches). To determine the cellular volume, the 'fill' option (threshold set at 0.010614749425259) was used.

Manual tracking of process tips

Manual tracking of the microglial process-tips was performed in ImageJ. For each clearly visible process, a trained observer set a point-ROI to the center of the process tip in each time-step and noted whether the process extended or retracted in that frame. From the point-ROI the coordinates were extracted using ImageJ. The speed of the extension or retraction was then determined as the displacement of the process tip between two consecutive time-steps.

Statistics

Statistical analysis was performed in GraphPad Prism, Version 9.3.1. All correlations (Fig. 5 d, e and Fig. 8i, j) have been tested for linearity (requirement for a Pearson correlation): A simple linear regression including a runs test was applied. No significant departure from linearity was detected for any correlation tested and thus, a Pearson correlation was used for all correlations. Column data sets (Fig. 8c-h) were tested for normal distribution using a D'Agostino & Pearson normality test. Not all conditions were normal distributed. Thus, a Mann-Whitney test was selected for statistical comparison.

Software and code availability

MotiQ source code and software, along with a Manual, are available online (https://github.com/hansenjn/MotiQ, license GPL-3.0).

Funding

This work was supported by grants from the German Science Foundation (EXC 1023 ImmunoSensation). This work was funded by the Deutsche Forschungsgemeinschaft (DFG, German Research Foundation) under Germany's Excellence Strategy -EXC2151-390873048.

Author Contributions Statement

J.N.H and A.H. conceived the study. J.N.H. developed software, performed experiments and analyzed data. M.B., M.J.P., M.P., H.B., M.S., L.F., K.R. performed experiments and analyzed data. J.F.J. supported software development and data analysis. I.F., G.C.P., D.B. and T.L. contributed reagents and methods. A.H. supervised the study. J.N.H. and A.H. wrote the manuscript with contribution from J.F.J. and G.C.P.

Acknowledgements

The authors thank Yvonne Biederbick and Antje Baumgartner for excellent technical assistance. The authors thank Dr. Luis Alvarez for helping with the visualization of the center of mass displacement over time in 3D.

Competing interests

The authors declare no conflict of interest.

References

Abdolhoseini, M, Walker, F, and Johnson, S (2016). Automated tracing of microglia using multilevel thresholding and minimum spanning trees. Annu Int Conf IEEE Eng Med Biol Soc 2016, 1208–1211.

Arganda-Carreras, I, Fernández-González, R, Muñoz-Barrutia, A, and Ortiz-De-Solorzano, C (2010). 3D reconstruction of histological sections: Application to mammary gland tissue. Microsc Res Tech 73, 1019–1029.

Arshadi, C, Günther, U, Eddison, M, Harrington, KIS, and Ferreira, TA (2021). SNT: a unifying toolbox for quantification of neuronal anatomy. Nat Methods 18, 374–377.

Badimon, A et al. (2020). Negative feedback control of neuronal activity by microglia. Nature 586, 417–423.

Baron, R, Babcock, AA, Nemirovsky, A, Finsen, B, and Monsonego, A (2014). Accelerated microglial pathology is associated with Aβ plaques in mouse models of Alzheimer's disease. Aging Cell 13, 584–595.

Basilico, B, Cortese, B, Ratano, P, Angelantonio, SD, and Ragozzino, D (2019). Time-lapse Whole-field Fluorescence Imaging of Microglia ProcessesMotility in Acute Mouse Hippocampal Slices and Analysis. Bio Protoc 9, e3220.

Bolmont, T, Haiss, F, Eicke, D, Radde, R, Mathis, CA, Klunk, WE, Kohsaka, S, Jucker, M, and Calhoun, ME (2008). Dynamics of the microglial/amyloid interaction indicate a role in plaque maintenance. J Neurosci 28, 4283–4292.

Cătălin, B, Stopper, L, Bălşeanu, T-A, and Scheller, A (2017). The in situ morphology of microglia is highly sensitive to the mode of tissue fixation. J Chem Neuroanat 86, 59–66.

Clausen, BE, Burkhardt, C, Reith, W, Renkawitz, R, and Förster, I (1999). Conditional gene targeting in macrophages and granulocytes using LysMcre mice. Transgenic Res 8, 265–277.

Condello, C, Yuan, P, Schain, A, and Grutzendler, J (2015). Microglia constitute a barrier that prevents neurotoxic protofibrillar Aβ42 hotspots around plaques. Nat Commun 6, 6176.

Conde, JR, and Streit, WJ (2006). Microglia in the aging brain. J Neuropathol Exp Neurol 65, 199–203.

Davalos, D, Grutzendler, J, Yang, G, Kim, JV, Zuo, Y, Jung, S, Littman, DR, Dustin, ML, and Gan, W-B (2005). ATP mediates rapid microglial response to local brain injury in vivo. Nat Neurosci 8, 752–758.

De Picker, LJ et al. (2021). Immune environment of the brain in schizophrenia and during the psychotic episode: A human post-mortem study. Brain Behav Immun 97, 319–327.

Dissing-Olesen, L, LeDue, JM, Rungta, RL, Hefendehl, JK, Choi, HB, and MacVicar, BA (2014). Activation of neuronal NMDA receptors triggers transient ATP-mediated microglial process outgrowth. J Neurosci 34, 10511–10527.

Erny, D et al. (2015). Host microbiota constantly control maturation and function of microglia in the CNS. Nat Neurosci 18, 965–977.

Fernández-Arjona, MDM, Grondona, JM, Granados-Durán, P, Fernández-Llebrez, P, and López-Ávalos, MD (2017). Microglia morphological categorization in a rat model of neuroinflammation by hierarchical cluster and principal components analysis. Front Cell Neurosci 11, 235.

Fontainhas, AM, Wang, M, Liang, KJ, Chen, S, Mettu, P, Damani, M, Fariss, RN, Li, W, and Wong, WT (2011). Microglial morphology and dynamic behavior is regulated by ionotropic glutamatergic and GABAergic neurotransmission. PLoS ONE 6, e15973.

Franco-Bocanegra, DK, Gourari, Y, McAuley, C, Chatelet, DS, Johnston, DA, Nicoll, JAR, and Boche, D (2021). Microglial morphology in Alzheimer's disease and after Aβ immunotherapy. Sci Rep 11, 15955.

Fülle, L et al. (2018). CCL17 exerts a neuroimmune modulatory function and is expressed in hippocampal neurons. Glia 66, 2246–2261.

Gyoneva, S, Davalos, D, Biswas, D, Swanger, SA, Garnier-Amblard, E, Loth, F, Akassoglou, K, and Traynelis, SF (2014). Systemic inflammation regulates microglial responses to tissue damage in vivo. Glia 62, 1345–1360.

Gyoneva, S, and Traynelis, SF (2013). Norepinephrine modulates the motility of resting and activated microglia via different adrenergic receptors. J Biol Chem 288, 15291–15302.

Haw, RTY, Tong, CK, Yew, A, Lee, HC, Phillips, JB, and Vidyadaran, S (2014). A three-dimensional collagen construct to model lipopolysaccharide-induced activation of BV2 microglia. J Neuroinflammation 11, 134.

Hefendehl, JK, Neher, JJ, Sühs, RB, Kohsaka, S, Skodras, A, and Jucker, M (2014). Homeostatic and injury-induced microglia behavior in the aging brain. Aging Cell 13, 60–69.

Honda, S, Sasaki, Y, Ohsawa, K, Imai, Y, Nakamura, Y, Inoue, K, and Kohsaka, S (2001). Extracellular ATP or ADP induce chemotaxis of cultured microglia through Gi/o-coupled P2Y receptors. J Neurosci 21, 1975–1982.

Hong, S, Dissing-Olesen, L, and Stevens, B (2016). New insights on the role of microglia in synaptic pruning in health and disease. Curr Opin Neurobiol 36, 128–134.

Jankowsky, JL, Xu, G, Fromholt, D, Gonzales, V, and Borchelt, DR (2003). Environmental enrichment exacerbates amyloid plaque formation in a transgenic mouse model of Alzheimer disease. J Neuropathol Exp Neurol 62, 1220–1227.

Jung, S, Aliberti, J, Graemmel, P, Sunshine, MJ, Kreutzberg, GW, Sher, A, and Littman, DR (2000). Analysis of fractalkine receptor CX(3)CR1 function by targeted deletion and green fluorescent protein reporter gene insertion. Mol Cell Biol 20, 4106–4114.

Kluge, MG, Kracht, L, Abdolhoseini, M, Ong, LK, Johnson, SJ, Nilsson, M, and Walker, FR (2017). Impaired microglia process dynamics post-stroke are specific to sites of secondary neurodegeneration. Glia 65, 1885–1899.

Koenigsknecht-Talboo, J, Meyer-Luehmann, M, Parsadanian, M, Garcia-Alloza, M, Finn, MB, Hyman, BT, Bacskai, BJ, and Holtzman, DM (2008). Rapid microglial response around amyloid pathology after systemic anti-Abeta antibody administration in PDAPP mice. J Neurosci 28, 14156–14164.

Koizumi, S, Shigemoto-Mogami, Y, Nasu-Tada, K, Shinozaki, Y, Ohsawa, K, Tsuda, M, Joshi, BV, Jacobson, KA, Kohsaka, S, and Inoue, K (2007). UDP acting at P2Y6 receptors is a mediator of microglial phagocytosis. Nature 446, 1091–1095.

Krabbe, G, Halle, A, Matyash, V, Rinnenthal, JL, Eom, GD, Bernhardt, U, Miller, KR, Prokop, S, Kettenmann, H, and Heppner, FL (2013). Functional impairment of microglia coincides with Beta-amyloid deposition in mice with Alzheimer-like pathology. PLoS ONE 8, e60921.

Kyriazis, AD et al. (2019). An End-to-end System for Automatic Characterization of Iba1 Immunopositive Microglia in Whole Slide Imaging. Neuroinformatics 17, 373–389.

Longair, MH, Baker, DA, and Armstrong, JD (2011). Simple Neurite Tracer: open source software for reconstruction, visualization and analysis of neuronal processes. Bioinformatics 27, 2453–2454.

Madry, C, Kyrargyri, V, Arancibia-Cárcamo, IL, Jolivet, R, Kohsaka, S, Bryan, RM, and Attwell, D (2018). Microglial Ramification, Surveillance, and Interleukin-1β Release Are Regulated by the Two-Pore Domain K+ Channel THIK-1. Neuron 97, 299-312.e6.

Matyash, M, Zabiegalov, O, Wendt, S, Matyash, V, and Kettenmann, H (2017). The adenosine generating enzymes CD39/CD73 control microglial processes ramification in the mouse brain. PLoS ONE 12, e0175012.

Merlini, M et al. (2021). Microglial Gi-dependent dynamics regulate brain network hyperexcitability. Nat Neurosci 24, 19–23.

Miyamoto, A, Wake, H, Ishikawa, AW, Eto, K, Shibata, K, Murakoshi, H, Koizumi, S, Moorhouse, AJ, Yoshimura, Y, and Nabekura, J (2016). Microglia contact induces synapse formation in developing somatosensory cortex. Nat Commun 7, 12540.

Nimmerjahn, A, Kirchhoff, F, and Helmchen, F (2005). Resting microglial cells are highly dynamic surveillants of brain parenchyma in vivo. Science 308, 1314–1318.

Ormel, PR et al. (2018). Microglia innately develop within cerebral organoids. Nat Commun 9, 4167.

Orr, AG, Orr, AL, Li, X-J, Gross, RE, and Traynelis, SF (2009). Adenosine A(2A) receptor mediates microglial process retraction. Nat Neurosci 12, 872–878.

Pagani, F et al. (2015). Defective microglial development in the hippocampus of Cx3cr1 deficient mice. Front Cell Neurosci 9, 111.

Paris, I, Savage, JC, Escobar, L, Abiega, O, Gagnon, S, Hui, C-W, Tremblay, M-È, Sierra, A, and Valero, J (2018). ProMoIJ: A new tool for automatic three-dimensional analysis of microglial process motility. Glia 66, 828–845.

Plescher, M, Seifert, G, Hansen, JN, Bedner, P, Steinhäuser, C, and Halle, A (2018). Plaque-dependent morphological and electrophysiological heterogeneity of microglia in an Alzheimer's disease mouse model. Glia 66, 1464–1480.

Riedl, J et al. (2010). Lifeact mice for studying F-actin dynamics. Nat Methods 7, 168–169.

Schmöle, A-C, Lundt, R, Toporowski, G, Hansen, JN, Beins, E, Halle, A, and Zimmer, A (2018). Cannabinoid Receptor 2-Deficiency Ameliorates Disease Symptoms in a Mouse Model with Alzheimer's Disease-Like Pathology. J Alzheimers Dis 64, 379–392.

Sipe, GO, Lowery, RL, Tremblay, MÈ, Kelly, EA, Lamantia, CE, and Majewska, AK (2016). Microglial P2Y12 is necessary for synaptic plasticity in mouse visual cortex. Nat Commun 7, 10905.

Sun, W, Suzuki, K, Toptunov, D, Stoyanov, S, Yuzaki, M, Khiroug, L, and Dityatev, A (2019). In vivo Two-Photon Imaging of Anesthesia-Specific Alterations in Microglial Surveillance and Photodamage-Directed Motility in Mouse Cortex. Front Neurosci 13, 421.

Takata, K et al. (2017). Induced-Pluripotent-Stem-Cell-Derived Primitive Macrophages Provide a Platform for Modeling Tissue-Resident Macrophage Differentiation and Function. Immunity 47, 183-198.e6.

Weinhard, L et al. (2018). Microglia remodel synapses by presynaptic trogocytosis and spine head filopodia induction. Nat Commun 9, 1228.

688 Young, K, and Morrison, H (2018). Quantifying Microglia Morphology from
689 Photomicrographs of Immunohistochemistry Prepared Tissue Using ImageJ. J Vis Exp.

690 Zariwala, HA, Borghuis, BG, Hoogland, TM, Madisen, L, Tian, L, De Zeeuw, CI, Zeng, H,
691 Looger, LL, Svoboda, K, and Chen, T-W (2012). A Cre-dependent GCaMP3 reporter mouse
692 for neuronal imaging in vivo. J Neurosci 32, 3131–3141.

693

694

Figure Legends

Figure 1: *MotiQ* workflow

MotiQ offers two main approaches for microglial cell analysis: **(a)** 2D time-lapse image analysis and **(b)** analysis of 3D time-lapse image stacks. Both workflows are comprised of three steps: single-cell selection with *MotiQ cropper*, image segmentation with *MotiQ thresholder*, and cell quantification using **(a)** *MotiQ 2D analyzer* or **(b)** *3D analyzer*. Cell volume, cell surface, cell skeleton, and the convex hull of the cell are reconstructed and analyzed and serve as a basis for the calculation of over 60 parameters of microglial morphology, dynamics, and fluorescence kinetics. MotiQ automatically generates 3D image visualizations by implementing *Volume Viewer* (ImageJ plugin by Kai Uwe Barthel). Scale bars = 20 µm.

Figure 2: Analysis of *in vivo* two-photon microscopy data

Selected morphological and dynamic parameters of a representative cortical microglial cell in CX3CR1$^{GFP/wt}$ mice imaged with *in vivo* two-photon microscopy and analyzed with *MotiQ*: **(a)** 2D ramification index, **(b)** 3D ramification index, **(c, d)** number of tips, number of branches and process tree length, **(e, f)** spanned area or spanned volume, and cell polarity vector length (5x magnified for better visualization), **(g, h)** shape dynamics and number of extensions and retractions as parameter for cell shape alteration, **(i, j)** scanned area or scanned volume represent the brain area or brain volume that has been occupied by a microglial cell over a selected time span (here 9 min).

Figure 3: Analysis of *ex vivo* two-photon microscopy data

2D and 3D analysis of microglial morphology and dynamics in *ex vivo* two-photon microscopy data of a representative microglial cell in acute cerebral slices of CX3CR1$^{EGFP/wt}$

mice before and after perfusion with 100 µM ATP (blue boxes). **(a, b)** Spanned area (2D) or volume (3D) before (t = 5 min) and during (t = 45 min) ATP perfusion. **(c, d)** Ramification index, **(e, f)** tree length, number of tips, and number of branches, **(g, h)** spanned area (2D) or volume (3D), cell polarity vector length, **(i, j)** shape dynamics, number of extensions and retractions, and **(k, l)** scanned area (2D) or volume (3D) during ATP perfusion. Scale bar, 20 µm.

Figure 4: Analysis of cellular morphology in tissue sections

(a, e, i) Maximum-intensity projections of confocal z stacks of an **(a)** Iba1-labeled murine cortical microglial cell, **(e)** Iba1-labeled murine retinal microglial cell, **(i)** hippocampal GFAP-labeled murine astrocyte, and **(m)** Iba1-labeled human microglial cell. 2D or 3D images of **(b, f, j, n)** reconstructed cell, **(c, g, k, o)** spanned volume (3D) or spanned area (2D), and **(d, h, l, p)** cell skeleton illustrating selected morphology parameters of **(a)**, **(e)** and **(i)** analyzed with *MotiQ*. Scale bars, 20 µm.

Figure 5: Fully automated analysis of cellular morphology in tissue sections

(a) Maximum-intensity projection of a confocal z stack of Iba1-labeled murine cortical microglia. Scale bar, 50 µm. **(b)** Maximum-intensity projection of automatically detected cells after analyzing (a) by *MotiQ 3D Analyzer* (using a high size threshold (of 10,000 voxels) to reconstruct cells that are moreover complete in the stack). **(c)** *MotiQ* visualizations of each cell: reconstructed cell (left), spanned volume (middle), and cell skeleton (right). Scale bars, 20 µm. **(d-e)** Direct comparison of the results obtained with *MotiQ* (c) to results obtained using **(d)** an alternative automated approach based on the commercial software Imaris or **(e)** a manual approach using the FIJI plugin Simple Neurite Tracer (Arshadi *et al.*, 2021). Each data point represents one cell. *MotiQ* results are indicated on the x-axis. Imaris (d) or manual tracing (e) results are indicated on the y-axis. Lines show mean and 95% confidence interval of a linear regression. r and p values for a Pearson correlation are indicated. Note: Imaris and

the manual approach did not allow to detect the upper right cell in the image (a), as the cell body is not completely within the stack. Thus, this cell is missing in the correlations.

Figure 6: Analysis of 2D- and 3D-cultured microglia

(a-f) *MotiQ* 2D analysis of epifluorescence time-lapse images of a representative primary microglial cell from CX3CR1$^{eGFP/+}$ mice, cultured in a 2D culture system. **(a)** False-colored fluorescence intensity images and **(b)** spanned area before (t = 0 min) and after (t = 11 min 30 sec) addition of ATP (100 µM). **(c)** Cell polarity, **(d)** shape dynamics, **(e)** scanned area, scanning activity, and **(f)** directionality (= accumulated/Euclidean center of mass displacement) of a selected microglial cell after addition of ATP. **(g-m)** *MotiQ* 3D analysis of spinning-disc confocal time-lapse images of a representative primary murine microglial cell from Lifeact–GFP$^{+/-}$ mice, cultured in a 3D Matrigel culture system. **(g)** Maximum-intensity projection images during baseline recording (t = 0 min) and ATP (t = 9 min 30 s) perfusion. **(h, i)** Spanned volume, **(i)** polarity vector, **(j)** 3D ramification index, **(k)** shape dynamics, **(l)** scanned area and scanning activity, and **(m)** directionality. Insets visualize selected measurements. Scale bar = 20 µm.

Figure 7: Correlative analysis of morphology, dynamics and fluorescence kinetics in cultured macrophages

MotiQ 2D analysis of epifluorescence time-lapse images of a 2D-cultured bone marrow-derived macrophage, expressing the genetically-encoded calcium sensor GCaMP3. **(a)** False-colored fluorescence intensity images before and during perfusion with ATP (5mM). Calcium signals were recorded for 90 seconds before perfusion with ATP (180 s) and wash-out. **(b, c)** Upon ATP perfusion, a calcium signal was detected and temporally correlated to changes in the cell's **(b)** 2D ramification index and **(c)** scanned area. Scale bar = 20 µm.

Figure 8: Analysis microglial morphology and dynamics in a cerebral amyloidosis mouse model of Alzheimer's disease

Analysis of microglial morphology and dynamics in *ex vivo* two-photon microscopy data of microglia in acute cerebral slices of APP/PS1 CX3CR1$^{EGFP/wt}$ mice or wild-type CX3CR1$^{EGFP/wt}$. **(a, b)** Maximum-intensity projection of images from **(a)** APP/PS1 CX3CR1$^{EGFP/wt}$ mice or **(b)** wild-type CX3CR1$^{EGFP/wt}$ mice. Scale bar, 50 µm. **(c)** Ramification index and **(d)** tree length, determined by *MotiQ 3D* analysis. **(e)** Shape dynamics and **(f)** scanned area, determined by *MotiQ 2D* analysis. **(g-j)** To verify the parameter results for shape dynamics and scanned area, for each analyzed cell, all visible processes were also manually tracked in 2D. Based on this tracking, for each cell, the average process speed of **(g)** process extensions or **(h)** retractions was determined. **(i-j)** Correlation of the manually determined process speeds with the *MotiQ* results shape dynamics (i, shape dynamics plotted alone in e) and scanned area (j, scanned area plotted alone in f). Bar plots (c-h) show the median ± interquartile range, individual data points represent individual cells (n = 3 animals per group; close: 9-14 cells per animal, distant: 14-17 cells per animal, wild-type: 10-13 cells per animal), p values for a two-sided Mann-Whitney test indicated. Data points in (i) and (j) also represent individual cells and are colored as in (c-h). Magenta: plaque-close cells. Purple: plaque-distance cells. Dark green: wild-type cells. Lines show mean and 95% confidence interval of a linear regression. r and p values for a Pearson correlation indicated.

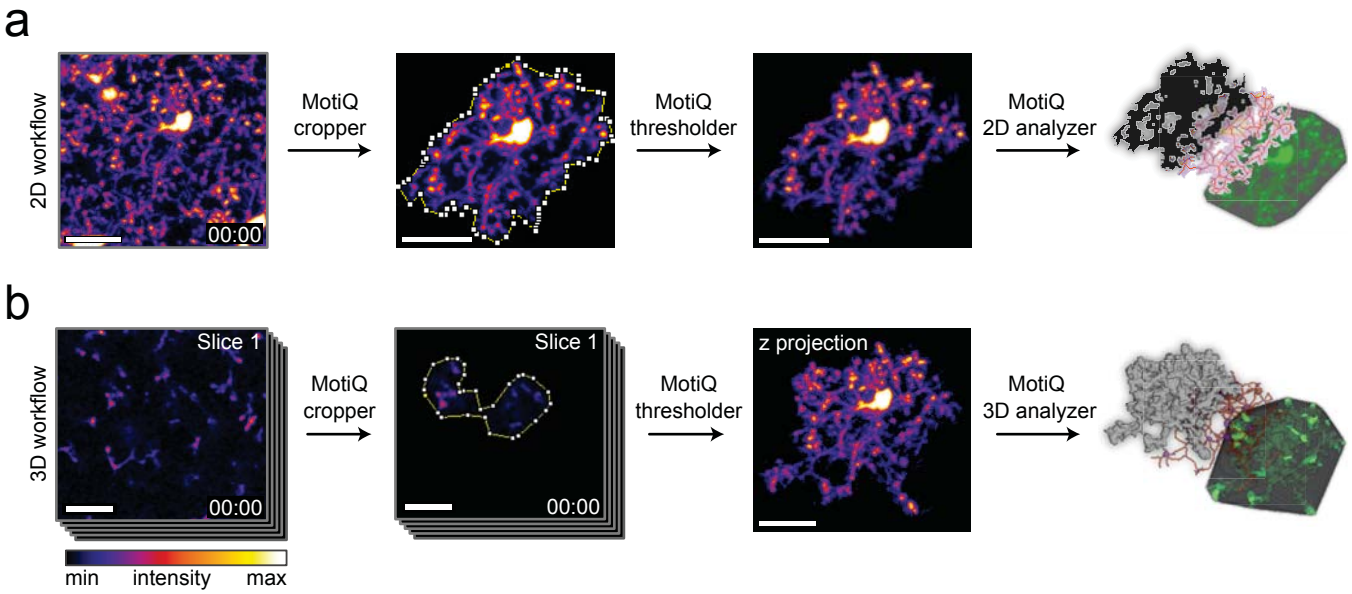
a
2D workflow
00:00
MotiQ
cropper
MotiQ
thresholder
MotiQ
2D analyzer
b
3D workflow
Slice 1
00:00
min
intensity
max
MotiQ
cropper
Slice 1
00:00
MotiQ
thresholder
z projection
MotiQ
3D analyzer

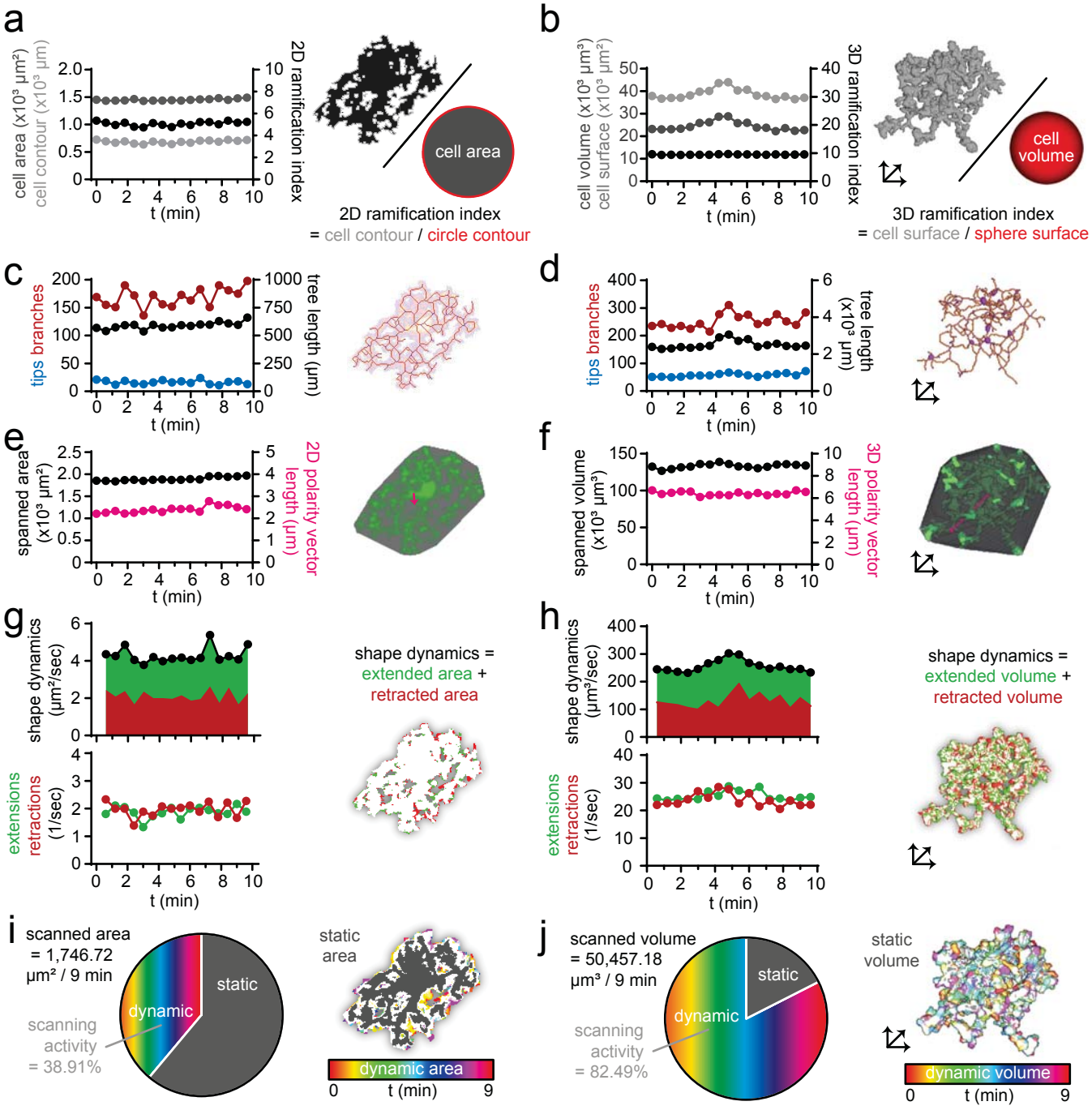
a
cell area (x10³ µm²)
cell contour (x10³ µm)
2D ramification index
t (min)
cell area
2D ramification index
= cell contour / circle contour
b
cell volume (x10³ µm³)
cell surface (x10³ µm²)
3D ramification index
t (min)
cell volume
3D ramification index
= cell surface / sphere surface
c
tips branches
tree length (µm)
t (min)
d
tips branches
tree length (x10³ µm)
t (min)
e
spanned area (x10³ µm²)
2D polarity vector length (µm)
t (min)
f
spanned volume (x10³ µm³)
3D polarity vector length (µm)
t (min)
g
shape dynamics (µm²/sec)
extensions retractions (1/sec)
t (min)
shape dynamics =
extended area +
retracted area
h
shape dynamics (µm³/sec)
extensions retractions (1/sec)
t (min)
shape dynamics =
extended volume +
retracted volume
i
scanned area
= 1,746.72
µm² / 9 min
static
dynamic
scanning activity
= 38.91%
static area
dynamic area
0
t (min)
9
j
scanned volume
= 50,457.18
µm³ / 9 min
static
dynamic
scanning activity
= 82.49%
static volume
dynamic volume
0
t (min)
9

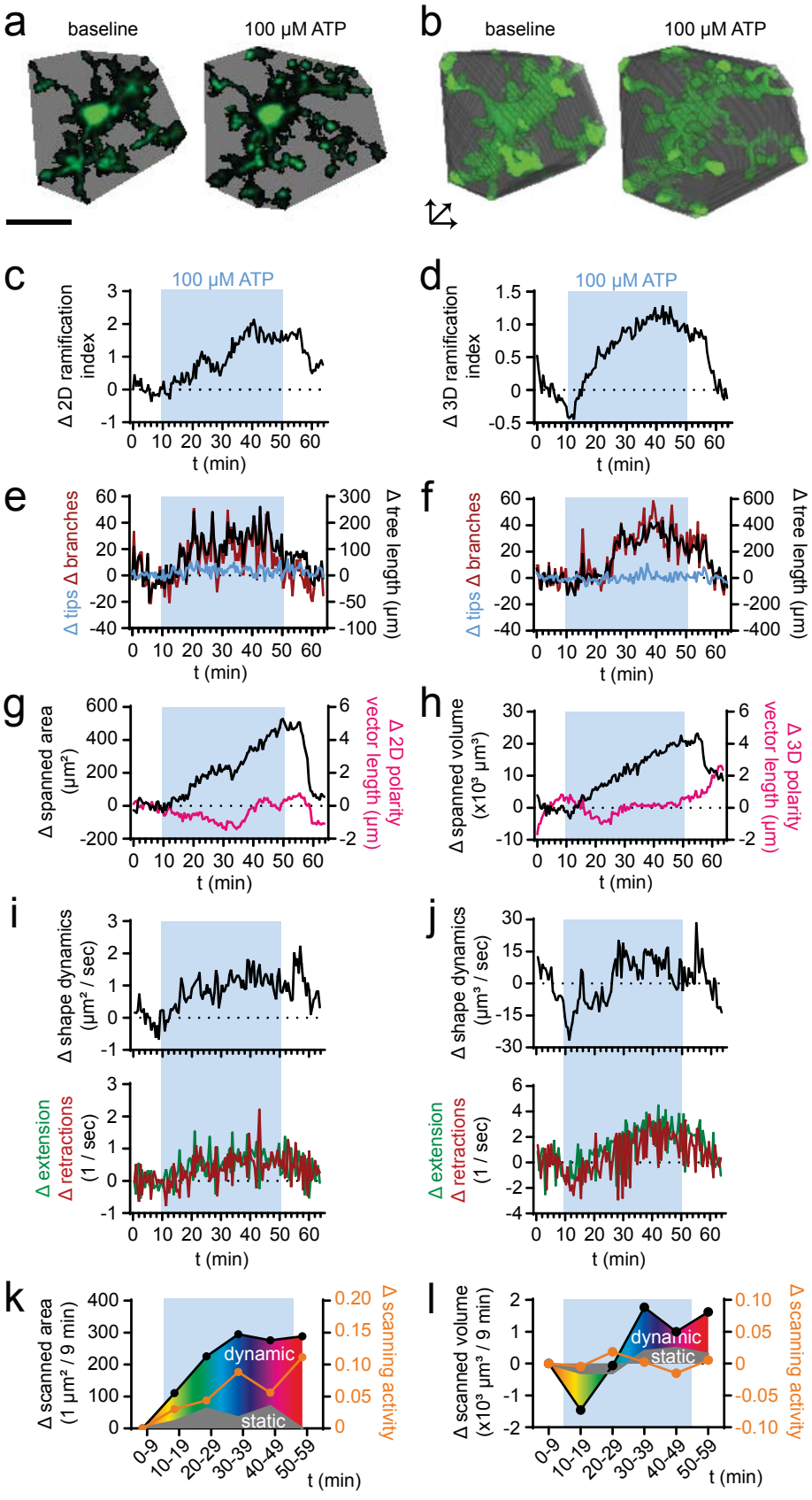
a
baseline
100 µM ATP
b
baseline
100 µM ATP
c
100 µM ATP
Δ 2D ramification index
t (min)
d
100 µM ATP
Δ 3D ramification index
t (min)
e
Δ tips Δ branches
Δ tree length (µm)
t (min)
f
Δ tips Δ branches
Δ tree length (µm)
t (min)
g
Δ spanned area (µm²)
Δ 2D polarity vector length (µm)
t (min)
h
Δ spanned volume (x10³ µm³)
Δ 3D polarity vector length (µm)
t (min)
i
Δ shape dynamics (µm² / sec)
Δ extension
Δ retractions
(1 / sec)
t (min)
j
Δ shape dynamics (µm³ / sec)
Δ extension
Δ retractions
(1 / sec)
t (min)
k
Δ scanned area (1 µm² / 9 min)
dynamic
static
Δ scanning activity
0-9
10-19
20-29
30-39
40-49
50-59
t (min)
l
Δ scanned volume (x10³ µm³ / 9 min)
dynamic
static
Δ scanning activity
0-9
10-19
20-29
30-39
40-49
50-59
t (min)

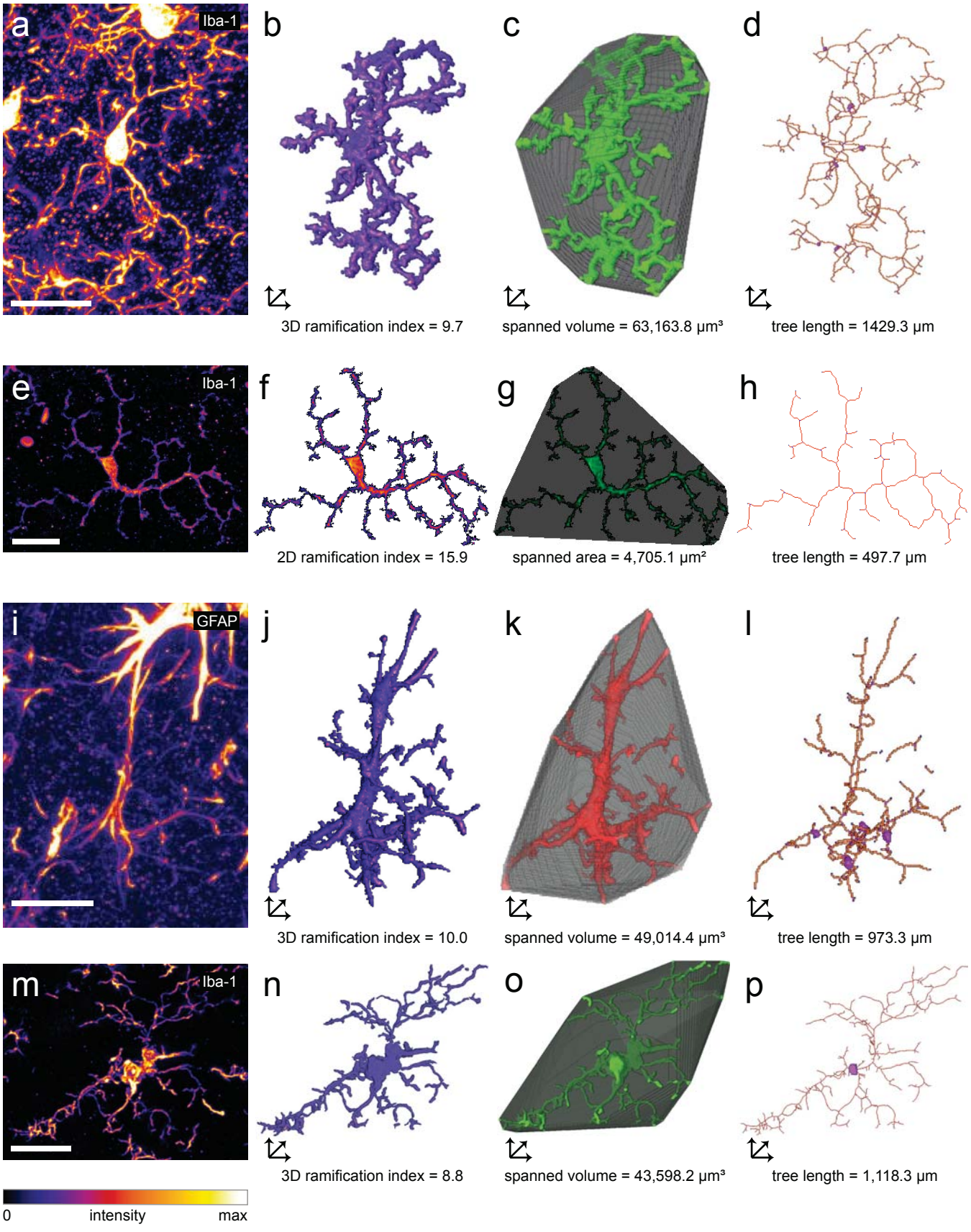
a
Iba-1
b
c
d
3D ramification index = 9.7
spanned volume = 63,163.8 µm³
tree length = 1429.3 µm
e
Iba-1
f
g
h
2D ramification index = 15.9
spanned area = 4,705.1 µm²
tree length = 497.7 µm
i
GFAP
j
k
l
3D ramification index = 10.0
spanned volume = 49,014.4 µm³
tree length = 973.3 µm
m
Iba-1
n
o
p
3D ramification index = 8.8
spanned volume = 43,598.2 µm³
tree length = 1,118.3 µm
0
intensity
max

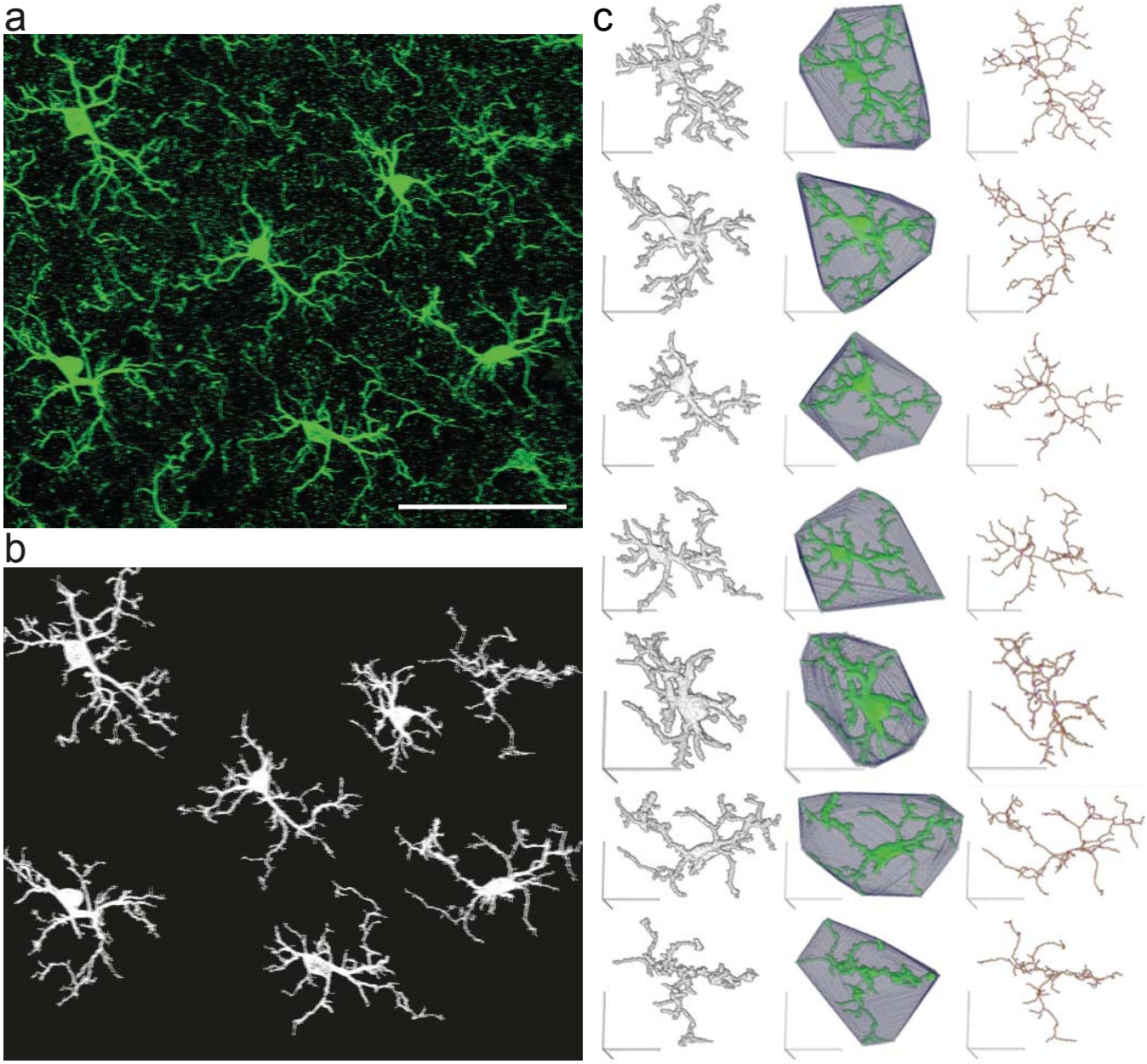
a
b
c
d
volume (x100 µm3)
surface (x1000 µm2)
branches (x10)
tips (x10)
tree length (x100 µm)
Imaris
r = 0.94
p = 6x10-3
r = 0.98
p = 6x10-4
r = 0.83
p = 0.04
r = 0.91
p = 0.01
r = 0.93
p = 7x10-3
e
volume (x100 µm3)
junctions
branches (x10)
tips (x10)
tree length (x100 µm)
Manual tracing
r = 0.96
p = 2x10-3
r = 0.88
p = 0.02
r = 0.87
p = 0.03
r = 0.81
p = 0.05
r = 0.95
p = 4x10-3
MotiQ

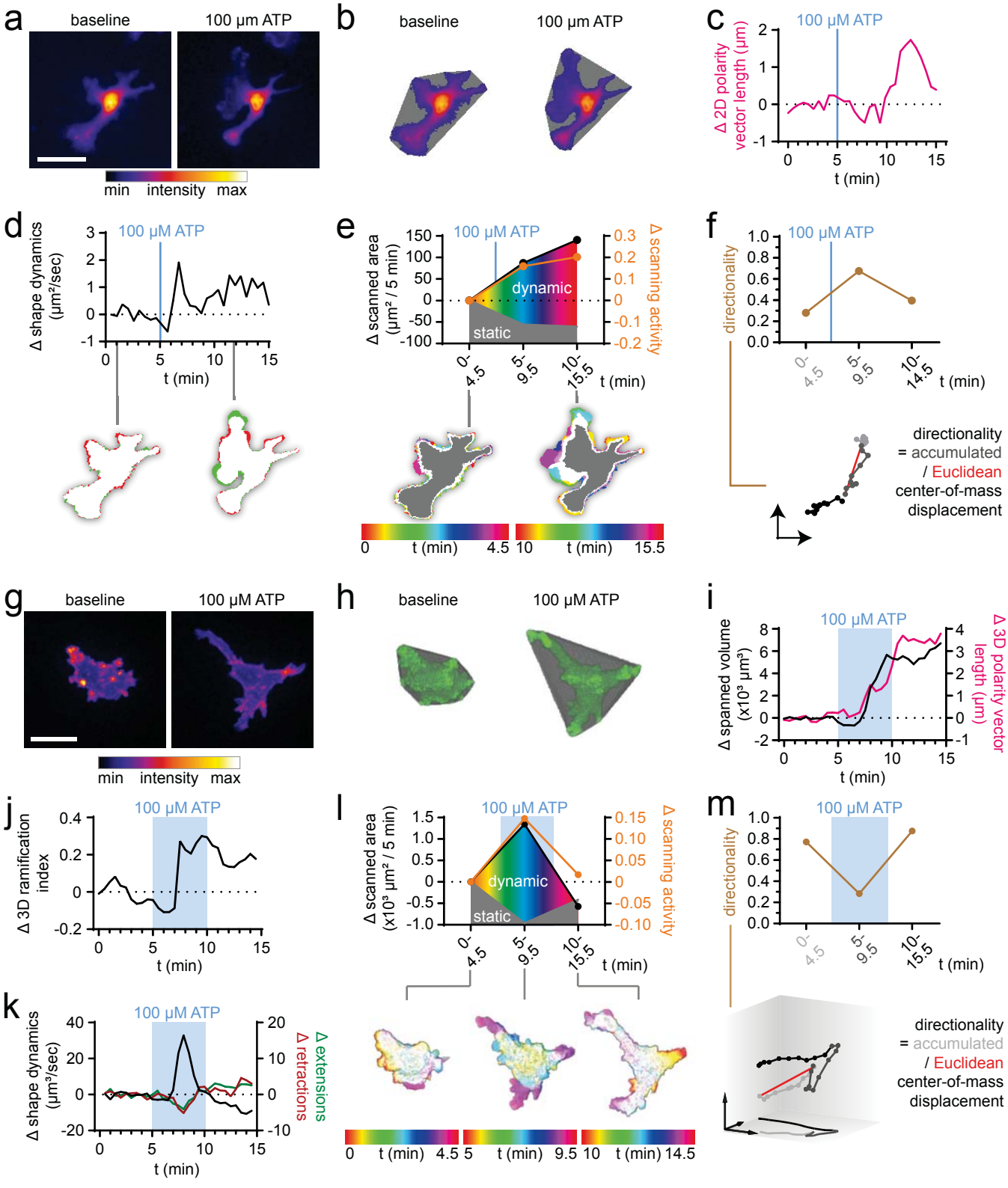
a
baseline
100 µm ATP
min intensity max
b
baseline
100 µm ATP
c
100 µM ATP
Δ 2D polarity vector length (µm)
t (min)
d
100 µM ATP
Δ shape dynamics (µm²/sec)
t (min)
e
100 µM ATP
Δ scanned area (µm² / 5 min)
Δ scanning activity
dynamic
static
t (min)
0 t (min) 4.5
10 t (min) 15.5
f
100 µM ATP
directionality
t (min)
directionality = accumulated / Euclidean center-of-mass displacement
g
baseline
100 µM ATP
min intensity max
h
baseline
100 µM ATP
i
100 µM ATP
Δ spanned volume (x10³ µm³)
Δ 3D polarity vector length (µm)
t (min)
j
100 µM ATP
Δ 3D ramification index
t (min)
k
100 µM ATP
Δ shape dynamics (µm³/sec)
Δ extensions
Δ retractions
t (min)
l
100 µM ATP
Δ scanned area (x10³ µm² / 5 min)
Δ scanning activity
dynamic
static
t (min)
0 t (min) 4.5
5 t (min) 9.5
10 t (min) 14.5
m
100 µM ATP
directionality
t (min)
directionality = accumulated / Euclidean center-of-mass displacement

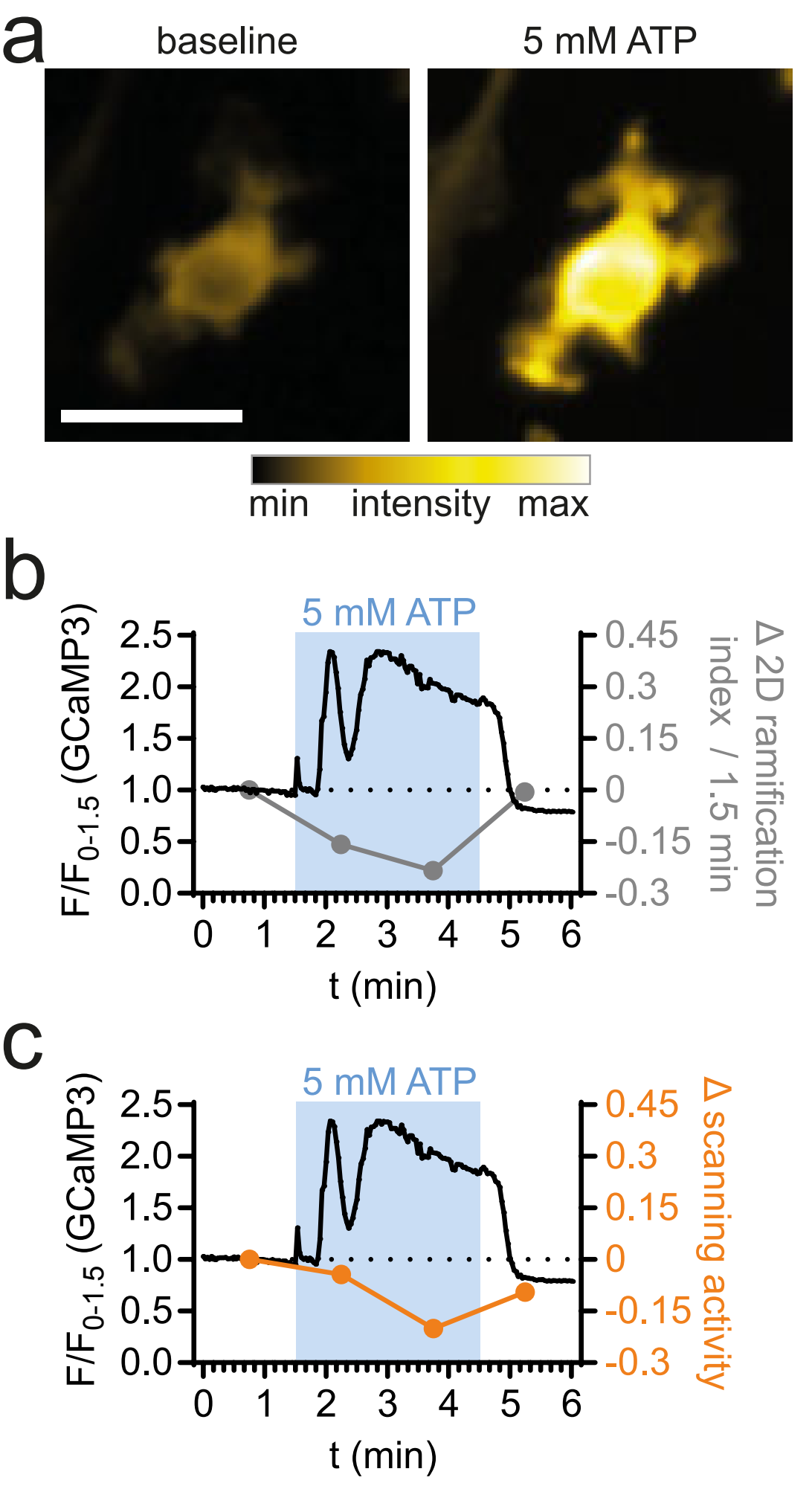
a
baseline
5 mM ATP
min
intensity
max
b
5 mM ATP
F/F0-1.5 (GCaMP3)
2.5
2.0
1.5
1.0
0.5
0.0
0
1
2
3
4
5
6
t (min)
0.45
0.3
0.15
0
-0.15
-0.3
Δ 2D ramification index / 1.5 min
c
5 mM ATP
F/F0-1.5 (GCaMP3)
2.5
2.0
1.5
1.0
0.5
0.0
0
1
2
3
4
5
6
t (min)
0.45
0.3
0.15
0
-0.15
-0.3
Δ scanning activity

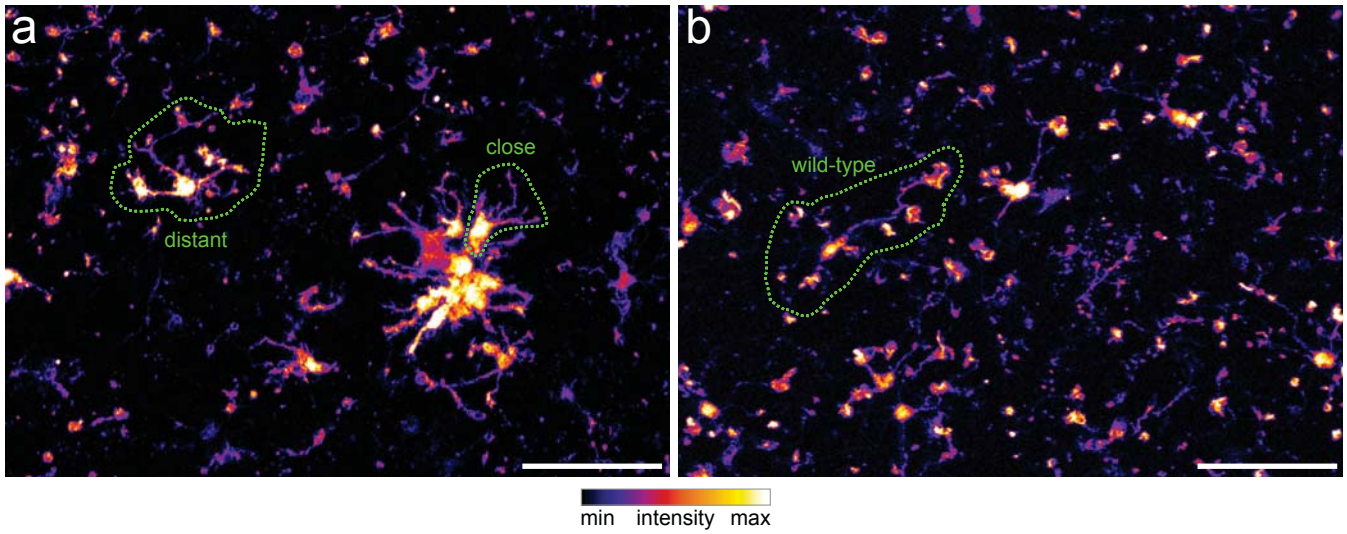
a
close
distant
b
wild-type
min
intensity
max

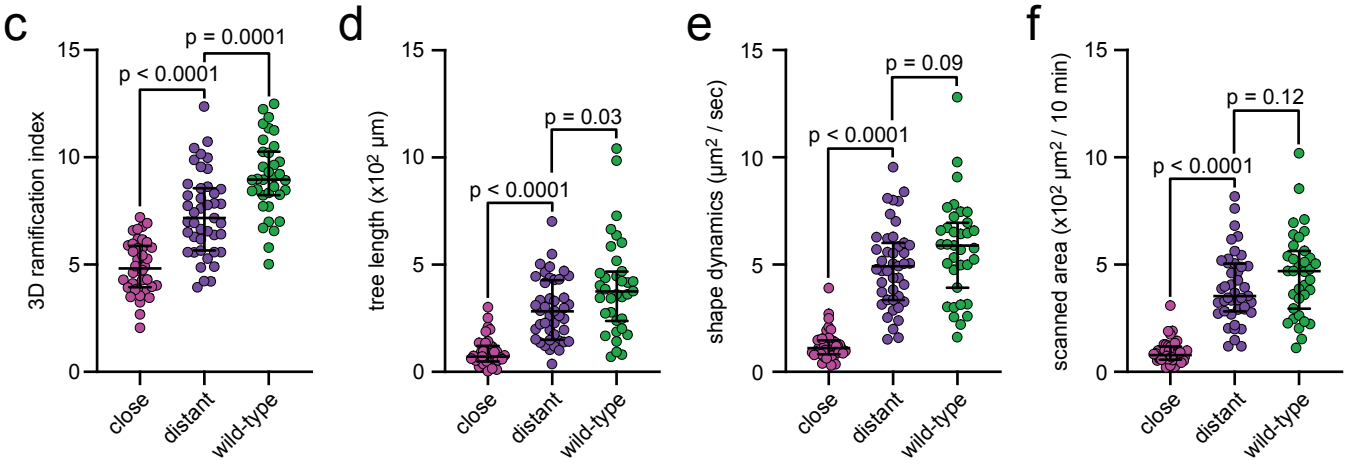
c
3D ramification index
p = 0.0001
p < 0.0001
d
tree length (x10² µm)
p = 0.03
p < 0.0001
e
shape dynamics (µm² / sec)
p = 0.09
p < 0.0001
f
scanned area (x10² µm² / 10 min)
p = 0.12
p < 0.0001
close
distant
wild-type

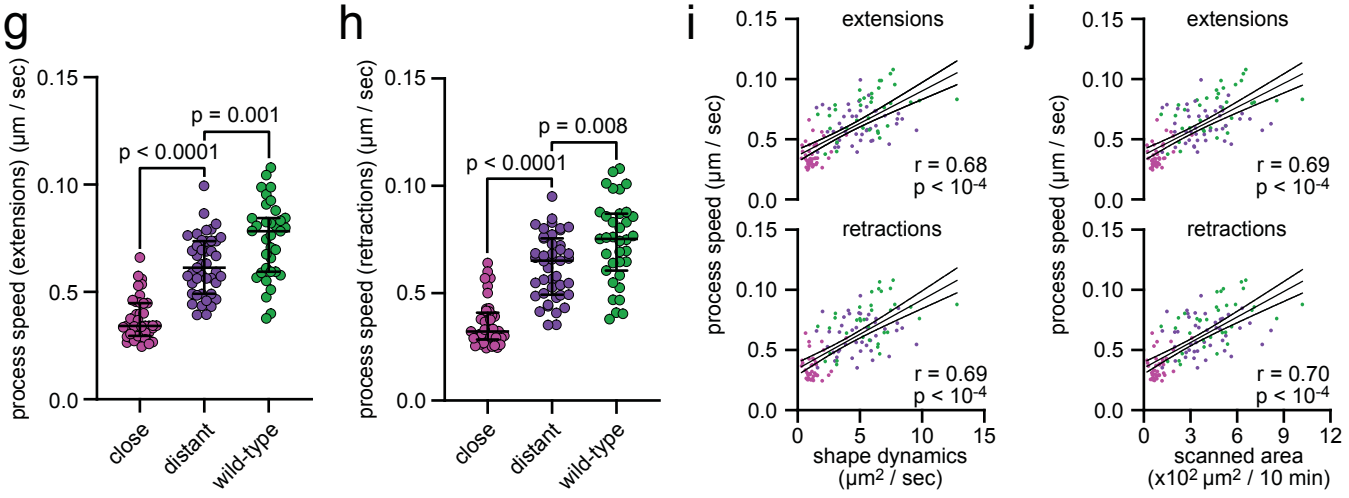
g
process speed (extensions) (µm / sec)
p = 0.001
p < 0.0001
h
process speed (retractions) (µm / sec)
p = 0.008
p < 0.0001
close
distant
wild-type
i
extensions
r = 0.68
p < 10-4
retractions
r = 0.69
p < 10-4
process speed (µm / sec)
shape dynamics
(µm² / sec)
j
extensions
r = 0.69
p < 10-4
retractions
r = 0.70
p < 10-4
process speed (µm / sec)
scanned area
(x10² µm² / 10 min)